

Geometry-aware similarity metrics for neural representations on Riemannian and statistical manifolds

N Alex Cayco Gajic^{1,†}, Arthur Pellegrino^{2,3,†}

[†] Equal contribution. Author order determined randomly.

1. *Département d'Etudes Cognitives, École Normale Supérieure – PSL*

2. *Gatsby Unit, University College London*

3. *Département d'Informatique, École Normale Supérieure – PSL*

Correspondence to: arthur.pellegrino@ens.fr

Abstract

Similarity measures are widely used to interpret the representational geometries used by neural networks to solve tasks. Yet, because existing methods compare the *extrinsic* geometry of representations in state space, rather than their *intrinsic* geometry, they may fail to capture subtle yet crucial distinctions between fundamentally different neural network solutions. Here, we introduce metric similarity analysis (MSA), a novel method which leverages tools from Riemannian geometry to compare the intrinsic geometry of neural representations under the manifold hypothesis. We show that MSA can be used to i) disentangle features of neural computations in deep networks with different learning regimes, ii) compare nonlinear dynamics, and iii) investigate diffusion models. Hence, we introduce a mathematically grounded and broadly applicable framework to understand the mechanisms behind neural computations by comparing their intrinsic geometries.

1 Introduction

Neural networks have historically been seen as “black-box” systems whose internal computations are inherently opaque. However, recent progress in mechanistic interpretability has led to broad efforts to reverse-engineer neural networks by analysing their weights and activations. These findings have revealed that subtle variations in initialization (Y. Li et al., 2015; Wang et al., 2018), architecture (Maheswaranathan et al., 2019), or learning regime (Chizat, Oyallon, and Bach, 2019; Jacot, Gabriel, and Hongler, 2018; Paccolat et al., 2021; Saxe, McClelland, and Ganguli, 2019; Woodworth et al., 2020) can produce different learned representations in otherwise similarly performant models. Importantly, such representational geometry has been shown to determine generalization properties (Chou et al., 2025; Johnston and Fusi, 2023; Q. Li, Sorscher, and Sompolinsky, 2024; Shang, Kreiman, and Sompolinsky, 2025; Woodworth et al., 2020). Understanding the internal mechanisms underlying a particular neural computation thus requires a principled way to contrast networks with potentially different architectures.

Towards this end, a multitude of similarity measures have been proposed to compare the hidden layer activations of neural networks (Klabunde et al., 2025). Widely used methods include linear regression, Procrustes, centred kernel alignment (CKA), canonical correlation analysis (CCA), representational similarity analysis (RSA), and their variants (Boix-Adsera et al., 2022; Grave, Joulin, and Berthet, 2019; Harvey, Lipshutz, and Williams, 2024; Kornblith

et al., 2019; Kriegeskorte, Mur, and Bandettini, 2008; Raghu et al., 2017; Williams et al., 2021). The core idea behind these methods is to align or correlate the representational geometries of hidden layer activations as they are embedded in state-space, to measure their similarity.

By focusing on the state-space geometries, these methods do not explicitly leverage the “manifold hypothesis”: the widely accepted view that input data lie on an intrinsically low-dimensional manifold (Tenenbaum, Silva, and Langford, 2000). An alternate approach instead examines neural network computations in terms of how they transform this input manifold. For example, successive layers in a deep network progressively warp the input manifold to extract task-relevant features. Such warping can be studied formally using tools from Riemannian geometry, both in neural networks (Brandon, Angus Chadwick, and Pellegrino, 2025; Hauser and Ray, 2017; Kaul and Lall, 2019; Poole et al., 2016), as well as in dynamical systems models (Pellegrino and Chadwick, 2025), where the input manifold is instead warped through time.

In this Riemannian view, the extrinsic geometry of a representation (e.g., its embedding) reflects less about internal computations than its intrinsic geometry, which characterises the pairwise relationships between points along the manifold. For example, a two-dimensional input may be embedded in ambient space as a flat plane or curved into a Swiss roll (Fig. 1). In this case, Procrustes or RSA will report high dissimilarity, despite all angles and distances *along* the manifolds being identical. Conversely, one can design embeddings that are highly similar extrinsically

but whose intrinsic geometries mismatch. In the following sections, we will show that neural networks can likewise exhibit substantial discrepancies between their intrinsic and extrinsic geometry. This illustrative example reveals the need for a Riemannian approach that targets the similarity of representations’ intrinsic geometries, not their embeddings.

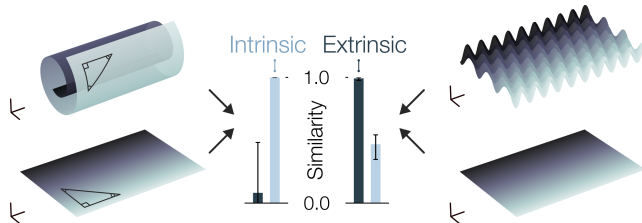


Fig. 1: *Intrinsic vs. extrinsic geometric similarity.*

To address this gap, we introduce **metric similarity analysis (MSA)**, a new framework to compare the intrinsic geometry of neural network computations from the lens of Riemannian geometry. We highlight MSA as a mathematically grounded method that satisfies the conditions to be a distance function defining a topological metric space over Riemannian metrics of a manifold.

Our theoretical contributions are:

1. **A Riemannian similarity measure.** MSA leverages the pullback metric to define a similarity between the exact intrinsic geometries of manifolds. We prove several mathematical results regarding MSA, including invariance to state-space rotations and choice of intrinsic coordinates.
2. **A novel distance between symmetric positive definite (SPD) matrices.** In order to compare Riemannian metrics arising from different representations, we propose the *spectral ratio* as a distance on the SPD cone that is well suited for similarity analysis.

We apply this theory to:

- **Rich and lazy learning.** We show that common methods report high similarity between rich and lazy deep networks, two learning regimes that are known to use different computational strategies. In contrast, MSA distinguishes clearly between rich vs. lazy representations.
- **Dynamical systems.** We train state-space models (SSMs) and recurrent neural networks (RNNs) on a sequence working memory task, and show that MSA uncovers differences in their internal computations.
- **Diffusion model.** In large-scale text-to-image diffusion models, we study how guidance affects latent diffusion dynamics by using MSA to compare the information geometries of their statistical manifolds.

Thus, we introduce a new framework anchored in Riemannian geometry, with which we show that identifying fundamentally distinct neural computations often requires uncovering minute differences in representational geometry.

Related work

Distances between representations. Similarity measures compare the hidden-layer activations of two networks $\varphi^1 : \mathbb{R}^{n_{in}} \rightarrow \mathbb{R}^{n_1}$ and $\varphi^2 : \mathbb{R}^{n_{in}} \rightarrow \mathbb{R}^{n_2}$ by defining a distance:

$$d(\varphi^1, \varphi^2) \geq 0$$

(or inversely, a similarity; see Klabunde et al. (2025) for a review). Methods such as CKA, CCA, RSA and Procrustes first sample the activations of each network given a finite set of k inputs: $M_1 = [\varphi^1(\mathbf{x}_1), \dots, \varphi^1(\mathbf{x}_k)]$ and $M_2 = [\varphi^2(\mathbf{x}_1), \dots, \varphi^2(\mathbf{x}_k)]$ for $\mathbf{x}_i \in \mathbb{R}^{n_{in}}$. The distance between φ^1 and φ^2 is treated as a distance between M_1 and M_2 as point clouds embedded in state space. For example, Procrustes finds the minimum distance over rotations of one point cloud to another: $d_{\text{Proc}}(M_1, M_2) = \min_{Q \in O(n)} \|M_1 - M_2 Q\|_F^2$. In this work, we do not perform any such sampling, and instead define a distance between the functions implemented by the networks using the pullback metrics of φ^1 and φ^2 . This enables an exact comparison of the intrinsic geometries of the manifolds, factoring out the embedding entirely.

Distances between nonlinear dynamics. A number of methods have recently been developed which go beyond static geometry to instead compare dynamical systems models, whether by learning diffeomorphic mappings between vector fields (Chen et al., 2024; Sagodi and I. M. Park, 2025), aligning Koopman modes in function space (Huang et al., 2025; Ostrow et al., 2023; Zhang et al., n.d.), or computing the Wasserstein distance between embeddings of local dynamics (Gosztolai et al., 2025). While MSA is not dynamics-specific, it can nonetheless be used to compare the geometry and dynamics of input-driven systems. Furthermore, its non-specificity enables comparison across model classes.

Riemannian geometry of neural networks. Riemannian geometry has numerous applications in machine learning, including: metric learning (Gruffaz and Sassen, 2025), natural gradients (Amari, 1998), mechanistic interpretability (Brandon, Angus Chadwick, and Pellegrino, 2025; Hauser and Ray, 2017; Pellegrino and Chadwick, 2025), and characterizing the latent space of deep generative models (Arvanitidis, Hansen, and Hauberg, 2017; Y.-H. Park et al., 2023; Shao, Kumar, and Thomas Fletcher, 2018). One recent paper applied information geometry to compare probabilistic models in the space of their predictions, i.e., outputs (Mao et al., 2024). However, MSA is the first method to define a Riemannian similarity measure on *hidden layer representations*. To this end, we introduce the spectral ratio (SR), a bounded distance on the SPD cone for similarity analysis. Unlike the classical affine-invariant Riemannian metric (AIRM), the boundedness of the SR guarantees similarities in $[0, 1]$. Nevertheless, it would be straightforward to define an AIRM-based variant of MSA, as has been done for RSA when comparing representational covariance matrices (Shahbazi et al., 2021).

2 Methods

In this section we define metric similarity analysis (MSA), which provides an exact comparison of neural representations under the manifold hypothesis. We begin by introducing a neural network as a mapping from an input manifold to a representational manifold in activation space. We then review the pullback metric as an exact characterization of the intrinsic geometry of this mapping at a point on the manifold. To compare two networks, we introduce the spectral ratio (SR): a new pseudodistance between SPD matrices using generalised eigenvalue theory. Finally, we provide a formal definition of MSA as the integrated SR over the input manifold, and demonstrate that it satisfies the conditions to induce a pseudometric space over Riemannian metrics.

Neural network model. We work in the general setting of a network mapping inputs on a manifold \mathcal{M} to target outputs. Symbolically, such a network can be summarised as:

$$\mathcal{M} \xrightarrow{\psi} \mathbb{R}^{n_{in}} \xrightarrow{\varphi} \mathbb{R}^n \xrightarrow{\zeta} \mathbb{R}^{n_{out}}$$

where ψ is the embedding of the input manifold, φ the network up to the hidden layer whose representation we wish to study, and ζ the subsequent layers and decoder. Many architectures such as multi-layer perceptrons, convolutional networks, and transformers fall within this setting. In section 3 we will show how MSA can be extended to dynamical systems, including state-space and diffusion models.

The pullback metric. The intrinsic geometry of a manifold is determined by a choice of inner product over its tangent spaces. To characterise our neural network, we will choose a particular intrinsic geometry on \mathcal{M} that captures how it is warped by $\varphi \circ \psi$. This can be done using the *pullback metric*, which defines the inner product between the tangent vectors of \mathcal{M} in terms of their corresponding dot product in \mathbb{R}^n when mapped to the hidden layer (Hauser and Ray, 2017; Lee, 2003). Letting $(\cdot)_*$ denote the pushforward, the pullback metric is the following map:

$$g_p : T_p\mathcal{M} \times T_p\mathcal{M} \xrightarrow{\psi_*} \mathbb{R}^{n_{in}} \times \mathbb{R}^{n_{in}} \xrightarrow{\varphi_*} \mathbb{R}^n \times \mathbb{R}^n \xrightarrow{\langle \cdot, \cdot \rangle} \mathbb{R}$$

where $T_p\mathcal{M}$ is the tangent space at point $p \in \mathcal{M}$. Intuitively, the pushforward maps tangent vectors of the abstract input manifold \mathcal{M} to tangent vectors of the hidden layer manifold $(\varphi \circ \psi)(\mathcal{M})$, where their inner product can be measured using the standard Euclidean dot product $\langle \cdot, \cdot \rangle$ (Fig. 2). This value can be taken as the inner product between the original tangent vectors in $T_p\mathcal{M}$, in order to define the same intrinsic geometry on \mathcal{M} as its image in the hidden layer activation.

In local coordinates, the pushforward at p can be represented by the Jacobian $J(p)$ of $\varphi \circ \psi$. Then the tangent vectors $\mathbf{v}_i \in T_p\mathcal{M}$ are pushed forward to $J(p)\mathbf{v}_i$ in the hidden layer, where their inner product is simply $(J(p)\mathbf{v}_i) \cdot (J(p)\mathbf{v}_j) = \mathbf{v}_i J(p)^T J(p) \mathbf{v}_j$. In this way, the pullback metric can be represented as $G(p) = J(p)^T J(p) \in$

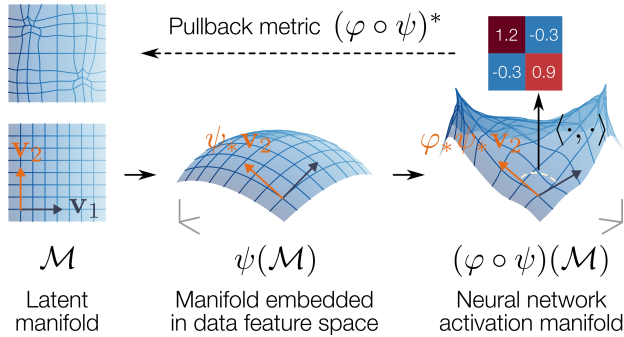


Fig. 2: *The pullback metric of neural representations.*

$\mathbb{R}^{m \times m}$ where $m = \dim(\mathcal{M})$. In particular, if the pushforward is injective, meaning that $(\varphi \circ \psi)(\mathcal{M})$ is an *immersion*, $G(p)$ is symmetric positive definite (SPD).

Several studies have shown that the geometry defined by $G(p)$ reflects the internal computations of deep networks (Brandon, Angus Chadwick, and Pellegrino, 2025; Hauser and Ray, 2017; Tennenholtz and Mannor, 2022). We may therefore expect that, for two different networks φ^1 and φ^2 receiving data from the same input manifold, comparing their respective pullback metrics $G^1(p)$ and $G^2(p)$ should provide a means of quantifying the similarity of their computations. This requires making a choice of distance function¹ between SPD matrices.

The spectral ratio of generalised eigenvalues. There exist distance functions on the space of SPD matrices (Förstner and Moonen, 2003; Lin, 2019). Such distance functions have for example been used to compare empirical covariance matrices, compute the KL divergence between Gaussian distributions, and define canonical correlations between data matrices. Here we introduce a novel distance function on SPD matrix space particularly suited for similarity analysis. Nevertheless, many of our mathematical results hold for general affine-invariant distance functions (App. A1).

DEFINITION 2.1 (Spectral ratio). Consider two SPD matrices $G, G' \in \mathbb{R}^{m \times m}$, and the generalised eigenequation $G\mathbf{v}_i = \lambda_i G'\mathbf{v}_i$. Here $\lambda_i \in \mathbb{R}_+$ and $\mathbf{v}_i \in \mathbb{R}^m$ form the i th generalised eigenvalue-eigenvector pair of (G', G) with $\lambda_{i+1} \leq \lambda_i$ for $i \in [m]$. We define the spectral ratio as:

$$d_{\text{SR}}(G, G') = 1 - \sqrt{\frac{\lambda_m}{\lambda_1}} \in [0, 1]$$

PROPOSITION 2.2 (The spectral ratio is a distance). *The SR is a pseudo-distance function on SPD matrices. This means that it satisfies i) separation: $d_{\text{SR}}(G, G) = 0$, ii) symmetry: $d_{\text{SR}}(G, G') = d_{\text{SR}}(G', G)$ and iii) the triangle inequality: $d_{\text{SR}}(G, G'') \leq d_{\text{SR}}(G, G') + d_{\text{SR}}(G', G'')$.* [PROOF]

Furthermore, since the spectral ratio is bounded, it can be

¹Distance functions are also called *metrics*, a concept that is related to – but not to be confused with – the *Riemannian metric*.

naturally used to define a similarity function:

$$1 - d_{\text{SR}}(G, G') \in [0, 1]$$

To gain intuition as to what this quantity represents we can consider two extreme cases. First, $1 - d_{\text{SR}}(G, G) = 1$. Second, if $\text{rank}(G) \neq \text{rank}(G')$, then $1 - d_{\text{SR}}(G, G') = 0$. Figure 3 shows the behaviour of this similarity function by comparing pairs of 2×2 SPD matrices generated by continuously varying the angle or the relative magnitudes among the columns of each matrix.

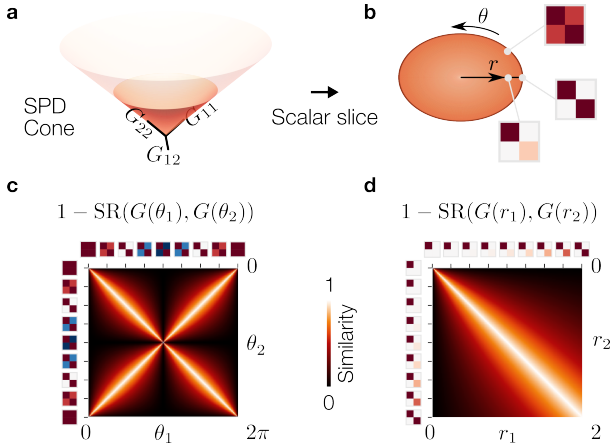


Fig. 3: *The spectral ratio is a distance over SPD matrices.* **a.** The set of SPD matrices (here 2×2) is a solid cone in the Euclidean space of their entries. **b.** Slice of the SPD cone along matrices which are related by a scalar multiple. The slice is characterised by a variable r , defining the relative magnitude of the diagonal entries and θ defining the magnitude of the off-diagonal entries. The spectral ratio defines a similarity between pairs of matrices on the SPD cone, with different relative θ (**c**) or r (**d**).

Metric Similarity Analysis (MSA). We have argued for using the pullback metric to characterize how the intrinsic geometry around a particular point $p \in \mathcal{M}$ is transformed by a neural network. Recall that for a specific choice of coordinate system, the pullback metric can be represented as an SPD matrix. Thus, we can compare two networks globally by integrating their spectral ratio over \mathcal{M} :

DEFINITION 2.3 (Metric similarity analysis). Let $G_p^{\varphi^1}$ and $G_p^{\varphi^2}$ the local coordinate representations of pullback metrics of the neural networks φ^1 and φ^2 , at a point p on an m -dimensional manifold \mathcal{M} . Then we define MSA as:

$$d_{\text{MSA}}(\varphi^1, \varphi^2) = \frac{1}{\text{Vol}_g(\mathcal{M})} \int_{\mathcal{M}} d_{\text{SR}}(G_p^{\varphi^1}, G_p^{\varphi^2}) d\text{vol}_g(p)$$

where the normalising factor $\text{Vol}_g(\mathcal{M})$ and integration over the volume form $d\text{vol}_g$ are dependent on the metric g on the input data manifold.

Just as the SR is a distance over SPD matrices, MSA defines a distance over Riemannian metrics.

PROPOSITION 2.4 (MSA is a distance over pullback Riemannian metrics). *MSA follows the separation, symmetry and triangle inequality identities.* [PROOF]

As for the SR, the MSA distance is bounded, and can be turned into a similarity function:

$$1 - d_{\text{MSA}}(\varphi^1, \varphi^2) \in [0, 1]$$

We use “MSA” to refer to either the distance or similarity function, depending on the context.

MSA provides a principled means of comparing the intrinsic geometries of neural network representations (Fig. 4). We will return to the mathematical properties of MSA in Section 4, where we show that it is invariant to the choice of coordinates on the manifold and to rotations in the neural network state space. In the next section, we demonstrate the applicability and relevance of MSA for comparing the intrinsic geometries of neural networks in various settings.

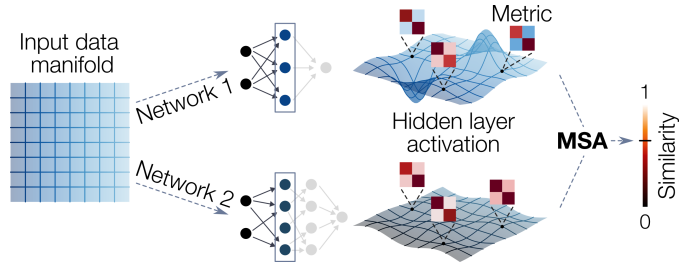


Fig. 4: *Metric similarity analysis enables comparison of the intrinsic geometry of neural representations.* Two neural networks receiving inputs from the same manifold with different hidden-layer geometries, corresponding to distinct Riemannian metrics.

3 Numerical experiments

Here, we highlight three key applications of MSA: i) revealing structural differences in the intrinsic geometry of deep network representations, ii) disentangling the computational mechanisms of different nonlinear dynamics architectures, and ii) comparing statistical manifolds in diffusion models.

MSA distinguishes rich and lazy representations

To highlight the importance of characterizing the *intrinsic* geometry of neural representations, we start by performing MSA on models known to produce different solutions to the same task: *rich* and *lazy* deep networks.

We trained a one-hidden-layer neural network to map inputs on a two-dimensional manifold to discrete classes (Fig. 5a). Specifically, we considered $\mathcal{M} = [-1, 1]^2$, with:

$$\mathbf{x} \in \mathcal{M}, \quad \mathbf{z} = \tanh(W_1 \mathbf{x}), \quad \mathbf{y} = W_2 \mathbf{z}$$

The network was trained using a cross entropy loss to map \mathbf{x} to a one-hot-encoded class vector:

$$\text{onehot}(\theta, k) = [\mathbb{1}_{\theta \in [0, 2\pi/k)}, \dots, \mathbb{1}_{\theta \in [2\pi - 2\pi/k, 2\pi)}]$$

where $\theta = \text{atan2}(\mathbf{x}) \in [0, 2\pi)$ and k is the number of classes.

Considerable prior work has shown that neural networks can perform such tasks via two fundamentally different

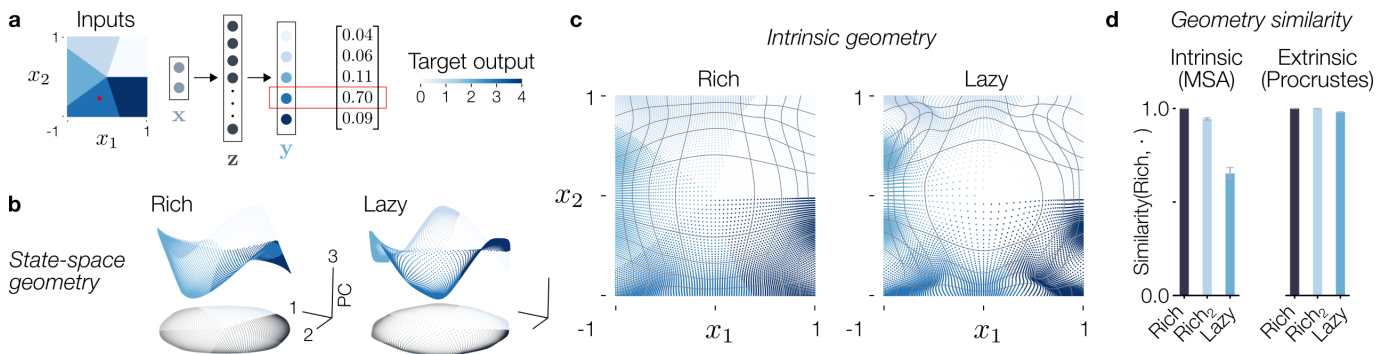


Fig. 5: **Rich and lazy network representations have different intrinsic geometries.** **a.** Network trained to map a 2D manifold to discrete classes. **b.** PCA applied to the activation of the rich and lazy network, coloured according to the target class. **c.** Mesh grid of the intrinsic geometry of the representations. **d.** Similarity between the rich and lazy representation; rich₂ is a different seed.

computational mechanisms. In the rich regime, networks learn latent features of their training data, leading to structured representations, whereas networks in the lazy regime overfit individual training data points (Woodworth et al., 2020). Small-variance weight initializations are known to produce rich learning, whereas large-variance initializations tend to lead to lazy learning (Saxe, McClelland, and Ganguli, 2013).

What representational geometries lie at the heart of these different computations? Simply visualizing the network activation in state space via principal component analysis (PCA) suggests a similar embedding geometry in each regime (Fig. 5b). In contrast, plotting the geodesic grid lines of the input manifold under the pullback metric hints at distinct intrinsic geometries, potentially supporting dif-

ferent network computations (Fig. 5c). To quantify this, we performed similarity analyses between the rich and lazy networks using both the intrinsic (via MSA) and extrinsic geometries (via Procrustes). Indeed, Procrustes reported near-perfect similarity between lazy and rich networks, whereas MSA reported low values compared to the similarity of the same regime across seeds (5d). Thus, characterizing the intrinsic geometry is necessary to disentangle fundamentally different computations in neural networks.

We next sought to exploit the fact that different hyperparameters generate divergent network solutions, due to different tasks (determined by the number of classes), learning regimes (by the variance of initial weights), or initializations (by the pseudo-random seed). To further test whether MSA can identify meaningful differences in network solutions, we varied these hyperparameters sequentially, forming a hierarchical structure (Fig. 6b). We then asked whether MSA identified similarities matching this hierarchy.

Indeed, MSA was able to capture this hierarchy, with similarities scaling evenly with the number of differing hyperparameters across models (Fig. 6a,b). In comparison, RSA was unable to distinguish between rich, lazy, and even untrained models. Importantly, both RSA and CCA reported intermediate similarity values for models with the fewest shared hyperparameters, with fundamentally different computations – for example when comparing trained vs. untrained models, or those trained on two vs. five classes. MSA, in contrast, found zero similarity in these cases.

These results demonstrate that MSA can disentangle finer-grained task-relevant structure than methods based purely on extrinsic geometry, enabling more meaningful comparisons between networks. In the next section, we will show that similar insights can be gained for nonlinear dynamics.

MSA enables the comparison of nonlinear dynamics

Here, we will show how MSA can be used to investigate dynamical systems models by examining how input manifolds are warped over time by nonlinear flows (Pellegrino

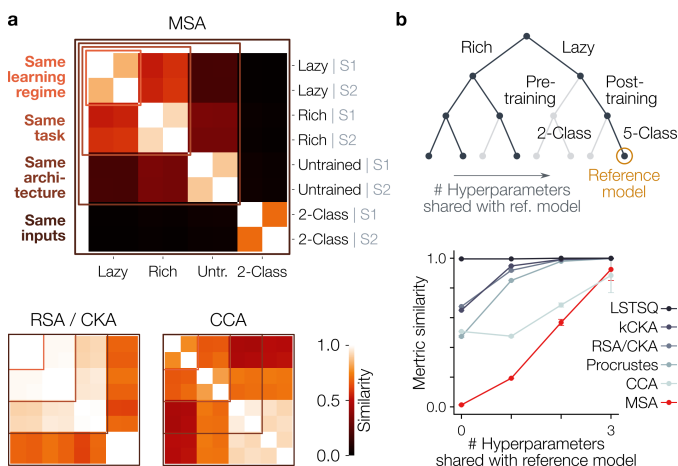


Fig. 6: **MSA captures hierarchical structure across neural representations.** Networks with different learning regimes, tasks, architectures, and seeds. **a.** MSA, RSA and CCA applied to pairs of these networks. Note that RSA and CKA are equivalent when mean-centered ($\bar{\cdot}$). MSA captures the hierarchical structure across models while CCA and RSA do not. **b.** Instead of considering all combinations of such hyperparameters, we hierarchically vary them. All networks receive the same input on a 2-dimensional planar manifold. They have different learning regimes (rich vs. lazy), or different tasks (5 vs. 2 classes), or seeds (S1/S2, defining initial weights).

and Chadwick, 2025). Specifically, we asked whether MSA could provide insight into the internal computations of dynamical systems models performing a task in which an internal memory of the input manifold must be maintained.

We trained models to reproduce an input sequence defined by two angles $\theta_1, \theta_2 \in \mathbb{S}^1$ following a variable delay (Fig. 7a). We considered two architectures commonly used in neuroscience applications: vanilla RNNs and structured SSMs (Durstewitz, Koppe, and Thurm, 2023; Ryoo et al., 2025). The dynamics of each model was governed by:

$$\begin{aligned} \text{RNN: } \quad & \frac{d}{dt} \mathbf{x}(t) = A \tanh(\mathbf{x}(t)) + B \mathbf{u}(t) \\ \text{SSM: } \quad & \frac{d}{dt} \mathbf{x}^{(i)}(t) = A^{(i)} \tanh(\mathbf{x}^{(i)}(t)) + B^{(i)} \mathbf{u}^{(i)}(t) \end{aligned}$$

where $\mathbf{u}(t) = \mathbf{u}^{(0)}(t) \in \mathbb{R}^3$ encodes the input angles and delay for each model (Fig. 7a). The SSM consisted of two blocks of dynamics ($i \in \{0, 1\}$) chained through a nonlinearity: $\mathbf{u}^{(1)}(t) = C^{(0)} \tanh(\mathbf{x}^{(0)}(t))$. The outputs were decoded from the hidden state: $\mathbf{y}(t) = C \mathbf{x}(t)$ and $\mathbf{y}(t) = C^{(1)}[\mathbf{x}^{(1)}(t), \mathbf{x}^{(2)}(t)]$ for the SSM and RNN, respectively. All A 's, B 's, and C 's were trainable parameters. The RNN weights were initialised to be Gaussian, while the SSM weights were initialised deterministically with HiPPO-LegS (Gu et al., 2022).

The input manifold for this task is a two-dimensional torus, $\mathcal{M} = \mathbb{T}^2 = \mathbb{S}^1 \times \mathbb{S}^1$ parametrised by θ_1 and θ_2 (Fig. 7b). After receiving the inputs, the model must maintain a representation of both angles in its internal state during the delay period. Multiple computational mechanisms have been proposed for such working memory tasks, from continuous attractors of fixed points (Khona and Fiete, 2022) to dynamical memories supported by non-normal dynamics (Ganguli, Huh, and Sompolinsky, 2008; Goldman, 2009). Importantly, the architecture biased the implemented mechanism: e.g. the SSM's block structure favoured non-normal dynamics. We thus asked whether the two models employ different computational strategies to perform the task.

We applied MSA to the full input-time manifolds produced by the RNN and the SSM. Specifically, we consider time as a separate coordinate, forming a 3-dimensional manifold \mathcal{M}' on which the 3×3 pullback metrics could be defined, enabling the geometry and dynamics of the models to be simultaneously compared. MSA was able to cluster the same architectures over seeds, while also identifying differences between trained and untrained models (Fig. 7c). To visualise these results we applied a variant of multi-dimensional scaling (MDS) on the MSA distance matrix, observing a low-dimensional representation that reflected the structure of the hyperparameters (architecture and training, Fig. 7d).

We asked whether it was possible to observe these differences through comparisons of the geometry or dynamics separately, by either applying RSA or DSA (Fig. 7e). While RSA was able to separate between the two trained

model architectures it was not sensitive to training stage, reporting the same similarity between the trained RNN vs. untrained SSM as the trained RNN vs. trained SSM (yellow vs. orange bars). DSA was even less sensitive to differences between the models. In contrast, MSA identified similarities that scaled both with architecture and training stage.

To see traces of the dynamic geometry within the models, we next applied MSA to compare the representation within the *same* model between timepoints t and t' (Fig. 7f). Interestingly, the two models showed different changes in their geometries over time, with only the RNN maintaining high similarity throughout the delay. These results echo recent work showing that linear dynamics can converge to non-normal rotational solutions (Ritter and Angus Chadwick, 2025), which could skew geometries due to shearing.

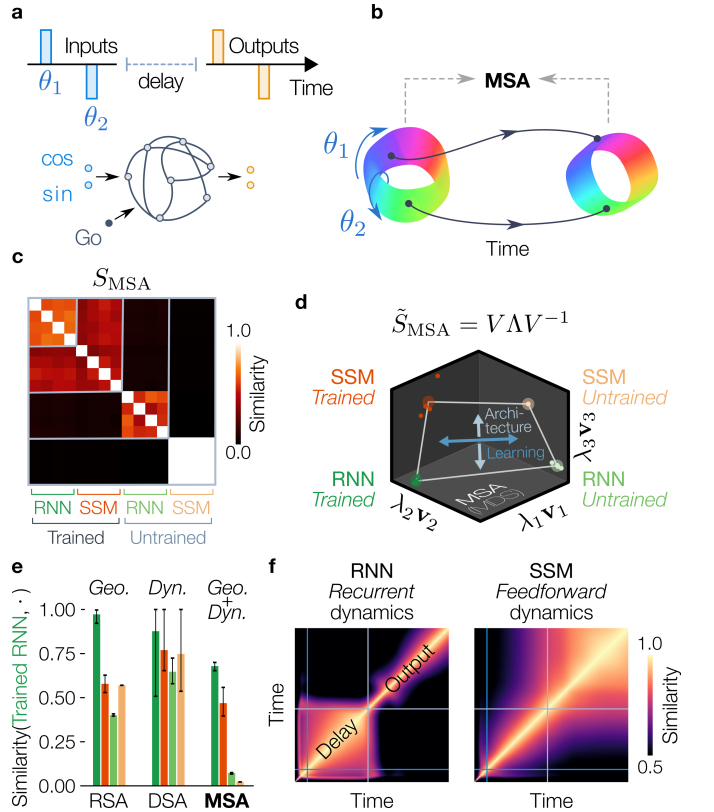


Fig. 7: **MSA enables comparing state-space models to recurrent neural networks.** **a.** The network receives a sequence of angular inputs: $u_i(t) = f_i(\theta_1)\mathbb{1}_{t=t_1} + f_i(\theta_2)\mathbb{1}_{t=t_2}$ for $i = 1, 2$, with $f_1(x) = \cos(x)$ and $f_2(x) = \sin(x)$, which it must keep in memory for a variable delay period. At the Go cue (signalled by $u_3(t) = \mathbb{1}_{t=t_{go}}$), it must output same sequence. **b.** PCA applied to the state of the RNN. **c.** MSA applied to the full input-time manifolds of different models. **d.** Eigenvectors of the doubly-centred pairwise MSA similarity matrix (i.e. MDS with MSA distance). **e.** Similarity of the geometry (RSA), dynamics (DSA) and geometry+dynamics (MSA) between the trained RNN and all other models. **f.** MSA applied to compare the representations within a single model at two timepoints (after the second input).

Together these results demonstrate how MSA reveals structural differences in dynamical representations of models while providing insight into their internal computations.

MSA extends to statistical manifold analysis

We next demonstrate how MSA can be extended to a probabilistic setting. We start by reviewing the link between the pullback and Fisher-Rao metrics, before applying MSA to generative text-to-image diffusion models.

Consider a statistical manifold \mathcal{M} whose points $\pi \in \mathcal{M}$ parametrise a probability density $p_\pi(\mathbf{x})$ over $\mathbf{x} \in \mathbb{R}^n$. For a given sample \mathbf{x} , the log-likelihood defines a map:

$$\mathcal{M} \xrightarrow{\log p_\pi(\cdot)} \mathbb{R}$$

whose pullback in local coordinates is $J_p(\pi)^\top J_p(\pi) \in \mathbb{R}^{m \times m}$, where $J_p(\pi) = (\nabla_\pi \log p_\pi(\mathbf{x}))^\top$. Taking an expectation over \mathbf{x} , we recover the Fisher information matrix:

$$F(\pi) = \mathbb{E}_{\mathbf{x} \sim p_\pi} [\nabla_\pi \log p_\pi(\mathbf{x}) \otimes \nabla_\pi \log p_\pi(\mathbf{x})] \in \mathbb{R}^{m \times m}$$

This SPD matrix defines the local coordinate expression of the Fisher-Rao metric, encoding changes in $p_\pi(\cdot)$ over \mathcal{M} .

We next show how MSA can compare the information geometries of diffusion models. A diffusion model is a backward-in-time stochastic differential equation (SDE):

$$d\mathbf{x} = \mathbf{f}(\mathbf{x}, \pi, t)dt + \sigma(t)dB, \quad \mathbf{x}(1) \sim \mathcal{N}(\mathbf{0}, I)$$

where B is a Brownian motion and $\pi \in \mathcal{M}$ is a variable that deterministically controls the diffusion process (e.g. a text prompt for conditional image generation). The model can be summarised as:

$$\mathbb{R}^n \xrightarrow{\varphi_\pi} \mathbb{R}^n, \quad \mathbf{x}(1) \rightarrow \mathbf{x}(0)$$

where φ_π is the flow of the system, and $\mathbf{x}(0)$ the generated sample (e.g. an image). This SDE is associated with a corresponding probability flow:

$$\partial_t p_\pi(\mathbf{x}, t) = -\nabla_{\mathbf{x}} \cdot (\mathbf{f}(\mathbf{x}, \pi, t)p_\pi(\mathbf{x}, t)) + \frac{1}{2}\sigma^2(t)\Delta_{\mathbf{x}}p_\pi(\mathbf{x}, t)$$

where $\nabla \cdot$ is the divergence, Δ the Laplacian, and $p_\pi(\mathbf{x}(1), 1) = \mathcal{N}(\mathbf{0}, I)$. Solving this flow at $p_\pi(\mathbf{x}(0), 0)$ gives the marginal density of the learned generative distribution of the SDE at $\mathbf{x}(0)$. Here we study the information geometry of this distribution over $\pi \in \mathcal{M}$.

Thanks to the scalability of MSA, we can apply it to StableDiffusionXL, a large text-to-image diffusion model capable of generating high quality images (Podell et al., 2023). The conditional variable π is the text embedding of the prompt such that the latent diffusion dynamics are given by:

$$d\mathbf{x} = \text{UNet}(\mathbf{x}, \text{TextEmb}(\text{"a leaf"}), t)dt + \sigma(t)dB$$

We defined a manifold \mathcal{M} of text embeddings via bilinear interpolation between four basis embeddings (Fig. 8b). This produces a statistical manifold with each $\pi \in \mathcal{M}$ corresponding to a different distribution of generated images. Using MSA we computed the similarity of the Fisher-Rao

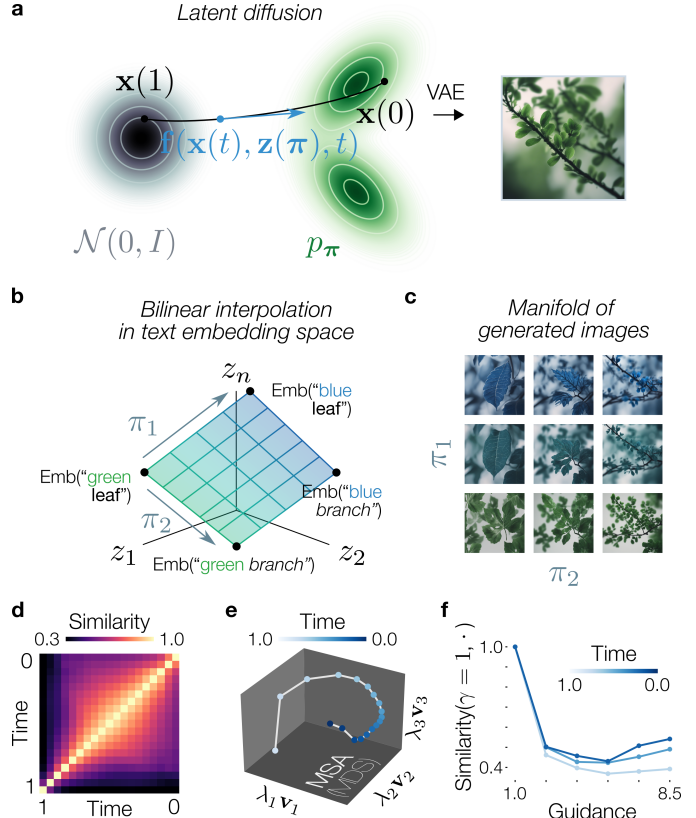


Fig. 8: *The latent space of diffusion models collapses without guidance.* **a.** Schematic of StableDiffusionXL: a backward diffusion process transports a Gaussian distribution to a latent generative distribution. Samples are then mapped to image space via a variational auto-encoder (VAE). **b.** The diffusion process is conditioned on a text embedding. We generated a manifold of text embeddings via bilinear interpolation: $\mathbf{z}(\pi) = \pi_1\pi_2\mathbf{v}_1 + (1-\pi_1)\pi_2\mathbf{v}_2 + \pi_1(1-\pi_2)\mathbf{v}_3 + (1-\pi_1)(1-\pi_2)\mathbf{v}_4$. This defines a statistical manifold of generative distributions. **c.** Samples across the manifold for a fixed $\mathbf{x}(1)$. **d.** Similarity between the statistical manifold geometry at any pair of time-point. **e.** Visualization of the information geometry using MDS on the MSA distance. **f.** MSA similarity between the statistical manifold at different guidance levels vs. no guidance ($\gamma = 1$).

metric at pairs of time points during the diffusion process, revealing dynamic changes in the intrinsic geometry throughout the flow (Fig. 8d). Furthermore, applying MDS on the MSA distance matrix enabled the trajectory of the information geometry to be visualized in a low-dimensional embedding (Fig. 8e).

Finally, MSA can be used to compare different diffusion dynamics, e.g., while varying hyperparameters. In particular, we studied how *guidance* affected the underlying information geometry. The guided diffusion dynamics are given by adding an estimation of the marginal score via an empty-string embedding:

$$d\mathbf{x} = (\gamma \text{UNet}(\mathbf{x}, \text{TextEmb}(\text{"a leaf"}), t) + (1 - \gamma) \text{UNet}(\mathbf{x}, \text{TextEmb}(\text{" "}), t))dt + \sigma(t)dB$$

Previous work has found empirically that the guidance

parameter γ controls a trade-off between image diversity and alignment-to-prompt (Ho and Salimans, 2022). To study this phenomenon at the level of the latent variable \mathbf{x} we computed the MSA similarity of models with different levels of guidance against the guidance-free model. We found that, past a certain γ , the geometry of the manifold became more similar to the guidance-free model, especially at times near 0. This hints at an optimal level γ where the information geometry of the learned generative distribution is most dissimilar to the guidance-free model, potentially aiding hyperparameter fine tuning.

4 Mathematical properties

In this section we briefly introduce two mathematical properties of MSA which are essential for it to be a well-defined similarity metric. First, a fundamental desideratum of any similarity measure is invariance to rotations. This is the case for many methods based on extrinsic geometry, such as CCA and Procrustes. MSA also satisfies this property.

PROPOSITION 4.1 (MSA is invariant to state-space rotations). *Consider two networks $\varphi^1 : \mathbb{R}^{n_{\text{in}}} \rightarrow \mathbb{R}^{n_1}$ and $\varphi^2 : \mathbb{R}^{n_{\text{in}}} \rightarrow \mathbb{R}^{n_2}$. Then:*

$$d_{\text{MSA}}(Q_1 \circ \varphi^1, Q_2 \circ \varphi^2) = d_{\text{MSA}}(\varphi^1, \varphi^2)$$

where $Q_i \in O(n_i)$ is an orthogonal matrix. [PROOF]

This invariance to rotations can be understood intuitively: given two tangent vectors $\mathbf{v}_1, \mathbf{v}_2 \in T_p \mathcal{M}$, composing the neural network functions with an orthogonal matrix Q (or any Euclidean isometry), will simply rotate the images of each \mathbf{v}_i under the pushforward, and thus will not change their dot product. Since the pullback metric is defined via this dot product, the intrinsic geometry remains the same.

A more subtle question, especially crucial for any method relying on Riemannian geometry, is whether MSA depends on the choice of local coordinates. In our numerical experiments we chose particular coordinates on the manifold aligned with the task variables. This in turn defined a coordinate representation of the metrics as matrices $G^{\varphi^1}(p)$, $G^{\varphi^2}(p)$ whose generalized eigenvalues we could then compute. However, changing the local coordinates will change these matrices, and therefore the solution to the generalised eigenvalue problem. Despite this, MSA itself remains invariant under such a change of local coordinates.

PROPOSITION 4.2 (MSA is invariant to changes in local coordinates). *Consider two networks $\varphi^1 : \mathbb{R}^{n_{\text{in}}} \rightarrow \mathbb{R}^{n_1}$, $\varphi^2 : \mathbb{R}^{n_{\text{in}}} \rightarrow \mathbb{R}^{n_2}$. Let (U_j, ϕ_j) and (U_k, ϕ_k) be smooth charts on \mathcal{M} . Then:*

$$d_{\text{MSA}}(\varphi^1 \circ \psi \circ f, \varphi^2 \circ \psi \circ f) = d_{\text{MSA}}(\varphi^1, \varphi^2)$$

where $f : \phi_k(U_k) \rightarrow \phi_j(U_j)$ is a diffeomorphism between the local coordinate chart domains. [PROOF]

These two key properties ensure that that MSA provides a meaningful distance between neural representations.

5 Discussion

We introduced a new similarity measure for comparing neural network solutions through their intrinsic geometries. At its most general, MSA defines a distance metric between Riemannian metrics over a manifold. In order to compare neural computations, we consider neural networks as functions that progressively warp an input manifold, whether from layer to layer or through time. Applying MSA to the pullback metrics of each network then provides a mathematically principled way to quantify the similarity of the networks' internal computations, rather than their extrinsic embedding geometries. We demonstrated the effectiveness of our approach in several examples of varying architecture, for static, dynamical, and generative models.

MSA requires a characterisation of the input data manifold. While this is straightforward to implement for most models, such a characterization can be challenging for applications to data where the manifold is not explicitly provided, e.g. in neuroscience data (Barbosa et al., 2025). This can be remedied by learning the manifold with a parametric model before applying MSA, as long as the data is sufficiently densely sampled. On the other hand, sampling-based methods such as Procrustes analysis and CCA work well even for sparsely sampled data. To this end, a natural extension of MSA to the data-poor regime would be to introduce a probabilistic model on the data sampling process.

A second limitation of MSA is that it does not capture how representations are used downstream. By focusing on the intrinsic geometry of a single hidden layer, MSA is agnostic as to how that information is exploited (or not) in later layers. For example, when the decoder layer is rank-deficient or low-dimensional, it may ignore part of the representational geometry, depending on how it is aligned with the nullspace. In contrast, several shape metrics have known connections with linear decoding (Harvey, Lipshutz, and Williams, 2024). Therefore a more complete characterization of network computations will likely require additional considerations of decoding.

Finally, our work remains mostly correlational. Similarity metrics do not offer causal insights into neural networks, only a geometric lens through which their computations can be interpreted. Nevertheless, similarity analysis can provide a useful tool for refining and manipulating models, for example, to identify new solutions (Qian and Pehlevan, 2025). Future work could attempt to directly manipulate the geometry of neural networks based on the insights gained from MSA to design more performant or robust models, offering a promising avenue for mechanistic interpretability.

Acknowledgments

We thank the Gatsby Unit for their feedback on this work. In particular, we are grateful to David O’Neill, whose results obtained during his Master’s at UCL inspired the development of MSA. We also thank the members of the Centre Sciences des Données at ENS for helpful discussions, especially Alexandre Vérine for insightful exchanges on the diffusion model section. This work was supported by the Agence National de Recherche (ANR-23-IACL-0008, ANR-17- 726 EURE-0017).

References

- Amari, Shun-Ichi (1998). “Natural gradient works efficiently in learning”. In: *Neural computation* 10.2, pp. 251–276.
- Arvanitidis, Georgios, Lars Kai Hansen, and Søren Hauberg (2017). “Latent space oddity: on the curvature of deep generative models. arXiv”. In: *Preprint posted online October 31*.
- Barbosa, Joao et al. (2025). “Quantifying Differences in Neural Population Activity With Shape Metrics”. In: *bioRxiv*, pp. 2025–01.
- Boix-Adsera, Enric et al. (2022). “GULP: a prediction-based metric between representations”. In: *Advances in Neural Information Processing Systems* 35, pp. 7115–7127.
- Brandon, Julian, Angus Chadwick, and Arthur Pellegrino (2025). “Emergent Riemannian geometry over learning discrete computations on continuous manifolds”. In: *arXiv preprint arXiv:2512.00196*.
- Chen, Ruiqi et al. (2024). “Dform: Diffeomorphic vector field alignment for assessing dynamics across learned models”. In: *arXiv preprint arXiv:2402.09735*.
- Chizat, Lenaïc, Edouard Oyallon, and Francis Bach (2019). “On lazy training in differentiable programming”. In: *Advances in neural information processing systems* 32.
- Chou, Chi-Ning et al. (2025). “Feature Learning beyond the Lazy-Rich Dichotomy: Insights from Representational Geometry”. In: *Forty-second International Conference on Machine Learning*.
- Durstewitz, Daniel, Georgia Koppe, and Max Ingo Thurm (2023). “Reconstructing computational system dynamics from neural data with recurrent neural networks”. In: *Nature Reviews Neuroscience* 24.11, pp. 693–710.
- Förstner, Wolfgang and Boudewijn Moonen (2003). “A metric for covariance matrices”. In: *Geodesy—the Challenge of the 3rd Millennium*. Springer, pp. 299–309.
- Ganguli, Surya, Dongsung Huh, and Haim Sompolinsky (2008). “Memory traces in dynamical systems”. In: *Proceedings of the national academy of sciences* 105.48, pp. 18970–18975.
- Goldman, Mark S (2009). “Memory without feedback in a neural network”. In: *Neuron* 61.4, pp. 621–634.
- Gosztolai, Adam et al. (2025). “MARBLE: interpretable representations of neural population dynamics using geometric deep learning”. In: *Nature Methods*, pp. 1–9.
- Grave, Edouard, Armand Joulin, and Quentin Berthet (2019). “Unsupervised alignment of embeddings with wasserstein procrustes”. In: *The 22nd International Conference on Artificial Intelligence and Statistics*. PMLR, pp. 1880–1890.
- Gruffaz, Samuel and Josua Sassen (2025). “Riemannian metric learning: Closer to you than you imagine”. In: *arXiv preprint arXiv:2503.05321*.
- Gu, Albert et al. (2022). “How to train your hippo: State space models with generalized orthogonal basis projections”. In: *arXiv preprint arXiv:2206.12037*.
- Harvey, Sarah E, David Lipshutz, and Alex H Williams (2024). “What representational similarity measures imply about decodable information”. In: *arXiv preprint arXiv:2411.08197*.
- Hauser, Michael and Asok Ray (2017). “Principles of Riemannian geometry in neural networks”. In: *Advances in neural information processing systems* 30.
- Ho, Jonathan and Tim Salimans (2022). “Classifier-free diffusion guidance”. In: *arXiv preprint arXiv:2207.12598*.
- Huang, Ann et al. (2025). “Inputdsa: Demixing then comparing recurrent and externally driven dynamics”. In: *arXiv preprint arXiv:2510.25943*.
- Jacot, Arthur, Franck Gabriel, and Clément Hongler (2018). “Neural tangent kernel: Convergence and generalization in neural networks”. In: *Advances in neural information processing systems* 31.
- Johnston, W Jeffrey and Stefano Fusi (2023). “Abstract representations emerge naturally in neural networks trained to perform multiple tasks”. In: *Nature Communications* 14.1, p. 1040.
- Kaul, Piyush and Brejesh Lall (2019). “Riemannian curvature of deep neural networks”. In: *IEEE transactions on neural networks and learning systems* 31.4, pp. 1410–1416.
- Khona, Mikail and Ila R Fiete (2022). “Attractor and integrator networks in the brain”. In: *Nature Reviews Neuroscience* 23.12, pp. 744–766.
- Klabunde, Max et al. (2025). “Similarity of neural network models: A survey of functional and representational measures”. In: *ACM Computing Surveys* 57.9, pp. 1–52.
- Kornblith, Simon et al. (2019). “Similarity of neural network representations revisited”. In: *International conference on machine learning*. PMLR, pp. 3519–3529.
- Kriegeskorte, Nikolaus, Marieke Mur, and Peter A Bandettini (2008). “Representational similarity analysis—connecting the branches of systems neuroscience”. In: *Frontiers in systems neuroscience* 2, p. 249.
- Lee, John M (2003). “Smooth manifolds”. In: *Introduction to smooth manifolds*. Springer, pp. 1–29.
- Li, Qianyi, Ben Sorscher, and Haim Sompolinsky (2024). “Representations and generalization in artificial and

- brain neural networks”. In: *Proceedings of the National Academy of Sciences* 121.27, e2311805121.
- Li, Yixuan et al. (2015). “Convergent learning: Do different neural networks learn the same representations?” In: *arXiv preprint arXiv:1511.07543*.
- Lin, Zhenhua (2019). “Riemannian geometry of symmetric positive definite matrices via Cholesky decomposition”. In: *SIAM Journal on Matrix Analysis and Applications* 40.4, pp. 1353–1370.
- Maheswaranathan, Niru et al. (2019). “Universality and individuality in neural dynamics across large populations of recurrent networks”. In: *Advances in neural information processing systems* 32.
- Mao, Jialin et al. (2024). “The training process of many deep networks explores the same low-dimensional manifold”. In: *Proceedings of the National Academy of Sciences* 121.12, e2310002121.
- Ostrow, Mitchell et al. (2023). “Beyond geometry: Comparing the temporal structure of computation in neural circuits with dynamical similarity analysis”. In: *Advances in Neural Information Processing Systems* 36, pp. 33824–33837.
- Paccolat, Jonas et al. (2021). “Geometric compression of invariant manifolds in neural networks”. In: *Journal of Statistical Mechanics: Theory and Experiment* 2021.4, p. 044001.
- Park, Yong-Hyun et al. (2023). “Understanding the latent space of diffusion models through the lens of riemannian geometry”. In: *Advances in Neural Information Processing Systems* 36, pp. 24129–24142.
- Pellegrino, Arthur and A Chadwick (2025). “RNNs perform task computations by warping neural representations”. In: *Advances in neural information processing systems* 38.
- Podell, Dustin et al. (2023). “Sdxl: Improving latent diffusion models for high-resolution image synthesis”. In: *arXiv preprint arXiv:2307.01952*.
- Poole, Ben et al. (2016). “Exponential expressivity in deep neural networks through transient chaos”. In: *Advances in neural information processing systems* 29.
- Qian, William and Cengiz Pehlevan (2025). “Discovering alternative solutions beyond the simplicity bias in recurrent neural networks”. In: *arXiv preprint arXiv:2509.21504*.
- Raghu, Maithra et al. (2017). “Svcca: Singular vector canonical correlation analysis for deep learning dynamics and interpretability”. In: *Advances in neural information processing systems* 30.
- Ritter, Laura and Angus Chadwick (2025). “Efficient Working Memory Maintenance via High-Dimensional Rotational Dynamics”. In: *bioRxiv*, pp. 2025–09.
- Ryoo, Avery Hee-Woon et al. (2025). “Generalizable, real-time neural decoding with hybrid state-space models”. In: *arXiv preprint arXiv:2506.05320*.
- Sagodi, Abel and Il Memming Park (2025). “Dynamical archetype analysis: Autonomous computation”. In: *arXiv preprint arXiv:2507.05505*.
- Saxe, Andrew M, James L McClelland, and Surya Ganguli (2013). “Exact solutions to the nonlinear dynamics of learning in deep linear neural networks”. In: *arXiv preprint arXiv:1312.6120*.
- (2019). “A mathematical theory of semantic development in deep neural networks”. In: *Proceedings of the National Academy of Sciences* 116.23, pp. 11537–11546.
- Shahbazi, Mahdiyar et al. (2021). “Using distance on the Riemannian manifold to compare representations in brain and in models”. In: *NeuroImage* 239, p. 118271.
- Shang, Jiaqi, Gabriel Kreiman, and Haim Sompolinsky (2025). “Unraveling the geometry of visual relational reasoning”. In: *ArXiv*, arXiv-2502.
- Shao, Hang, Abhishek Kumar, and P Thomas Fletcher (2018). “The riemannian geometry of deep generative models”. In: *Proceedings of the IEEE Conference on Computer Vision and Pattern Recognition Workshops*, pp. 315–323.
- Tenenbaum, Joshua B, Vin de Silva, and John C Langford (2000). “A global geometric framework for nonlinear dimensionality reduction”. In: *science* 290.5500, pp. 2319–2323.
- Tennenholtz, Guy and Shie Mannor (2022). “Uncertainty estimation using riemannian model dynamics for offline reinforcement learning”. In: *Advances in Neural Information Processing Systems* 35, pp. 19008–19021.
- Wang, Liwei et al. (2018). “Towards understanding learning representations: To what extent do different neural networks learn the same representation”. In: *Advances in neural information processing systems* 31.
- Williams, Alex H (2024). “Equivalence between representational similarity analysis, centered kernel alignment, and canonical correlations analysis”. In: *bioRxiv*, pp. 2024–10.
- Williams, Alex H et al. (2021). “Generalized shape metrics on neural representations”. In: *Advances in neural information processing systems* 34, pp. 4738–4750.
- Woodworth, Blake et al. (2020). “Kernel and rich regimes in overparametrized models”. In: *Conference on Learning Theory*. PMLR, pp. 3635–3673.
- Zhang, Shimin et al. (n.d.). “KoopSTD: Reliable Similarity Analysis between Dynamical Systems via Approximating Koopman Spectrum with Timescale Decoupling”. In: *Forty-second International Conference on Machine Learning*.

APPENDIX

A1 Metric similarity analysis

Pseudodistance function

Proof of proposition 2.2. Let $G, G', G'' \in \mathbb{R}^{m \times m}$ be positive definite matrices. We will denote $\lambda_i^{(G, G')}$ to be the i th generalized eigenvalue of G and G' with corresponding eigenvector $\mathbf{v}_i^{(G, G')}$, satisfying:

$$G\mathbf{v}_i^{(G, G')} = \lambda_i^{(G, G')} G' \mathbf{v}_i^{(G, G')}.$$

By convention we order the eigenvalues from largest to smallest:

$$\lambda_1^{(G, G')} \geq \dots \geq \lambda_m^{(G, G')} > 0.$$

A useful fact will be that the generalized eigenvalues of (G, G') and (AG, AG') are equal for any nonsingular $A \in \mathbb{R}^{m \times m}$. This follows from multiplying the equation above by A , i.e.: $AG\mathbf{v}_i^{(G, G')} = \lambda_i^{(G, G')} AG' \mathbf{v}_i^{(G, G')}$, therefore:

$$\lambda_i^{(AG, AG')} = \lambda_i^{(G, G')} \Rightarrow d_{\text{SR}}(AG, AG') = d_{\text{SR}}(G, G')$$

In particular, if we choose $A = (G')^{-1}$, we obtain the standard eigenvalue equation for the matrix $(G')^{-1}G$ with $\lambda_i^{(G, G')} = \lambda_i^{((G')^{-1}G, \mathbb{I})}$.

1. *Separation:* In this case, $\lambda_i^{(G, G)} = \lambda_i^{(G^{-1}G, \mathbb{I})} = \lambda_i^{(\mathbb{I}, \mathbb{I})} = 1$. Therefore, $d_{\text{SR}}(G, G) = 1 - \sqrt{\frac{1}{1}} = 0$.
2. *Symmetry:* Each generalized eigenvalue for (G, G') corresponds to a generalized eigenvalue for (G', G) . Since the eigenvalues are nonzero:

$$G\mathbf{v}_i^{(G, G')} = \lambda_i^{(G, G')} G' \mathbf{v}_i^{(G, G')} \Rightarrow \frac{1}{\lambda_i^{(G, G')}} G\mathbf{v}_i^{(G, G')} = G' \mathbf{v}_i^{(G, G')}$$

Since we define the generalized eigenvalues in decreasing order of magnitude, this means $\lambda_i^{(G', G)} = 1/(\lambda_{m-i+1}^{(G, G')})$. Thus,

$$d_{\text{SR}}(G', G) = 1 - \sqrt{\frac{\lambda_m^{(G', G)}}{\lambda_1^{(G', G)}}} = 1 - \sqrt{\frac{1/(\lambda_1^{(G, G')})}{1/(\lambda_m^{(G, G')})}} = 1 - \sqrt{\frac{\lambda_m^{(G, G')}}{\lambda_1^{(G, G')}}} = d_{\text{SR}}(G, G').$$

3. *Triangle inequality:* We start by defining $\Delta d_{\text{SR}} = d_{\text{SR}}(G, G') + d_{\text{SR}}(G', G'') - d_{\text{SR}}(G, G'')$. It then suffices to prove that $\Delta d_{\text{SR}} \geq 0$. So far we have shown that the spectral ratio is symmetric and invariant under left-multiplication by invertible matrices. Using these properties, we can rewrite:

$$\begin{aligned} \Delta d_{\text{SR}} &= d_{\text{SR}}(G, G') + d_{\text{SR}}(G'', G') - d_{\text{SR}}(G, G'') \\ &= d_{\text{SR}}(\underbrace{(G')^{-1}G, \mathbb{I}}_{:=\tilde{G}}) + d_{\text{SR}}(\underbrace{(G')^{-1}G'', \mathbb{I}}_{:=\tilde{G}''}) - d_{\text{SR}}(\underbrace{(G')^{-1}G, (G')^{-1}G''}_{:=\tilde{G}, \tilde{G}''}) \end{aligned}$$

To prove that $\Delta d_{\text{SR}} \geq 0$ we will need to understand how the standard eigenvalues of \tilde{G} and \tilde{G}'' relate to their generalized eigenvalues. For clarity we write $\mathbf{v}_i = \mathbf{v}_i^{(\tilde{G}, \tilde{G}'')}$ for the remainder of the proof. Then, we can write the generalized eigenvalues as:

$$\tilde{G}\mathbf{v}_i = \lambda_i^{(\tilde{G}, \tilde{G}'')} \tilde{G}'' \mathbf{v}_i \Rightarrow \lambda_i^{(\tilde{G}, \tilde{G}'')} = \frac{\mathbf{v}_i^\top \tilde{G} \mathbf{v}_i}{\mathbf{v}_i^\top \tilde{G}'' \mathbf{v}_i} = \frac{R(\tilde{G}, \mathbf{v}_i)}{R(\tilde{G}'', \mathbf{v}_i)}$$

where $R(A, \mathbf{v})$ is the Rayleigh quotient. Then, the spectral ratio distance can be written in terms of Rayleigh quotients:

$$d_{\text{SR}}(\tilde{G}, \tilde{G}'') = 1 - \sqrt{\frac{R(\tilde{G}, \mathbf{v}_m)}{R(\tilde{G}'', \mathbf{v}_m)} \cdot \frac{R(\tilde{G}'', \mathbf{v}_1)}{R(\tilde{G}, \mathbf{v}_1)}}$$

Recall that the Rayleigh quotient is bounded by above and below by the standard eigenvalues: $\lambda_m^{(A, \mathbb{I})} \leq R(A, \mathbf{v}) \leq$

$\lambda_1^{(A, \mathbb{I})}$ for any \mathbf{v} . We can use this to bound the ratio of Rayleigh quotients:

$$\frac{R(\tilde{G}, \mathbf{v}_m)}{R(\tilde{G}'', \mathbf{v}_m)} \cdot \frac{R(\tilde{G}'', \mathbf{v}_1)}{R(\tilde{G}, \mathbf{v}_1)} \geq \frac{\lambda_m^{(\tilde{G}, \mathbb{I})}}{\lambda_1^{(\tilde{G}'', \mathbb{I})}} \cdot \frac{\lambda_m^{(\tilde{G}'', \mathbb{I})}}{\lambda_1^{(\tilde{G}, \mathbb{I})}} = \frac{b}{a} \cdot \frac{b''}{a''}$$

where we have defined the following quantities for clarity:

$$a = \sqrt{\lambda_1^{(\tilde{G}, \mathbb{I})}}, \quad b = \sqrt{\lambda_m^{(\tilde{G}, \mathbb{I})}}$$

$$a'' = \sqrt{\lambda_1^{(\tilde{G}'', \mathbb{I})}}, \quad b'' = \sqrt{\lambda_m^{(\tilde{G}'', \mathbb{I})}}$$

Putting it all together, we can write (or bound) all three terms in Δd_{SR} as:

$$d_{\text{SR}}(\tilde{G}, \mathbb{I}) = 1 - \frac{b}{a}$$

$$d_{\text{SR}}(\tilde{G}'', \mathbb{I}) = 1 - \frac{b''}{a''}$$

$$d_{\text{SR}}(\tilde{G}, \tilde{G}'') \leq 1 - \frac{b}{a} \cdot \frac{b''}{a''}$$

Finally, since $b/a \leq 1$ and $b''/a'' \leq 1$,

$$0 \leq \left(1 - \frac{b}{a}\right) \left(1 - \frac{b''}{a''}\right)$$

$$= 1 - \frac{b}{a} - \frac{b''}{a''} + \frac{b}{a} \cdot \frac{b''}{a''}$$

$$= \left(1 - \frac{b}{a}\right) + \left(1 - \frac{b''}{a''}\right) - \left(1 - \frac{b}{a} \cdot \frac{b''}{a''}\right)$$

$$\leq d_{\text{SR}}(\tilde{G}, \mathbb{I}) + d_{\text{SR}}(\tilde{G}'', \mathbb{I}) + d_{\text{SR}}(\tilde{G}, \tilde{G}'') = \Delta d_{\text{SR}},$$

which concludes the proof. □

Proof of proposition 2.4. The *separation* and *symmetry* immediately follow from Proposition 2.2 and the linearity of integration over a manifold. As for the *triangle inequality*:

$$\begin{aligned} \Delta d_{\text{MSA}} &= d_{\text{MSA}}(\varphi^1, \varphi^2) + d_{\text{MSA}}(\varphi^2, \varphi^3) - d_{\text{MSA}}(\varphi^1, \varphi^3) \\ &= \frac{1}{v} \int_{\mathcal{M}} d_{\text{SR}}(G^{\varphi^1}, G^{\varphi^2}) + d_{\text{SR}}(G^{\varphi^2}, G^{\varphi^3}) - d_{\text{SR}}(G^{\varphi^1}, G^{\varphi^3}) dV(p) \\ &= \frac{1}{v} \int_{\mathcal{M}} \Delta d_{\text{SR}}(p) dV(p). \end{aligned}$$

In the proof of Proposition 2.2 we show that $\Delta d_{\text{SR}} \geq 0$, and the integral of a non-negative number is itself non-negative. Hence:

$$0 \leq \Delta d_{\text{MSA}} \iff d_{\text{MSA}}(\varphi^1, \varphi^3) \leq d_{\text{MSA}}(\varphi^1, \varphi^2) + d_{\text{MSA}}(\varphi^2, \varphi^3). \quad \square$$

Invariances properties

Proof of proposition 4.1. It suffices to show that the metric itself is invariant to state-space rotation. We consider a network $\varphi^i : \mathbb{R}^{n_{\text{in}}} \rightarrow \mathbb{R}^{n_i}$ with m -dimensional input manifold \mathcal{M} embedded through the mapping $\psi : \mathcal{M} \rightarrow \mathbb{R}^{n_{\text{in}}}$. Let (U, ϕ) be a smooth chart on \mathcal{M} where $U \subset \mathcal{M}$ is an open set with $\phi : U \rightarrow \phi(U) \subseteq \mathbb{R}^m$ a diffeomorphism. The pullback metric at $p \in U$ can be expressed in local coordinates as the following product of Jacobians:

$$G^{\varphi^i}(p) = J_{\varphi^i \circ \psi \circ \phi^{-1}}^\top J_{\varphi^i \circ \psi \circ \phi^{-1}} = J_{\psi \circ \phi^{-1}}^\top J_{\varphi^i}^\top J_{\varphi^i} J_{\psi \circ \phi^{-1}}$$

Let $\tilde{G}^{\varphi^i}(p)$ be the corresponding metric after rotating in state space by $Q_i \in O(n_i)$. Then:

$$\begin{aligned} \tilde{G}^{\varphi^i}(p) &= J_{Q_i \circ \varphi^i \circ \psi \circ \phi^{-1}}^\top J_{Q_i \circ \varphi^i \circ \psi \circ \phi^{-1}} \\ &= J_{\psi \circ \phi^{-1}}^\top J_{\varphi^i}^\top Q_i^\top Q_i J_{\varphi^i} J_{\psi \circ \phi^{-1}} \end{aligned}$$

$$= J_{\psi \circ \phi^{-1}}^\top J_{\varphi^i}^\top J_{\varphi^i} J_{\psi \circ \phi^{-1}} = G^{\varphi^i}(p)$$

Where $J_f(p)$ is the Jacobian of the function f evaluated at p . Thus:

$$\begin{aligned} d_{\text{MSA}}(Q_1 \circ \varphi^1, Q_2 \circ \varphi^2) &= \frac{1}{v} \int_{\mathcal{M}} d_{\text{SR}}(\tilde{G}^{\varphi^1}(p), \tilde{G}^{\varphi^2}(p)) dV(p) \\ &= \frac{1}{v} \int_{\mathcal{M}} d_{\text{SR}}(G^{\varphi^1}(p), G^{\varphi^2}(p)) dV(p) = d_{\text{MSA}}(\varphi^1, \varphi^2) \end{aligned}$$

Hence MSA is invariant to neural network hidden-layer state-space rotations. \square

This result can be viewed as a special case of a more general proposition: MSA is invariant to state-space transformations which are point-wise isometries with respect to the Euclidean dot product. The proof follows mutatis mutandis, with $\tilde{G}^{\varphi^i}(p)$ the metric under the isometry.

We note that these arguments do not rely on having networks with the same hidden layer sizes, as they can be independently rotated. We can get a stronger invariance if we assume that both neural networks are simultaneously acted upon by the same transformation. So far we have considered invariances to transformations of the hidden-layer state-space, but MSA is also invariant to simultaneous transformations of the input manifold, and in particular changes of local coordinates.

Proof of proposition 4.2. We consider two networks $\varphi^1 : \mathbb{R}^{m_{\text{in}}} \rightarrow \mathbb{R}^{n_1}$, $\varphi^2 : \mathbb{R}^{m_{\text{in}}} \rightarrow \mathbb{R}^{n_2}$, with m -dimensional input manifold \mathcal{M} embedded through the mapping $\psi : \mathcal{M} \rightarrow \mathbb{R}^{m_{\text{in}}}$. Let (U_j, ϕ_j) and (U_k, ϕ_k) be two smooth charts on \mathcal{M} where $U_j, U_k \subset \mathcal{M}$ are open sets with $U_j \cap U_k \neq \emptyset$ and $\phi_j : U_j \rightarrow \phi_j(U_j) \subseteq \mathbb{R}^m$, $\phi_k : U_k \rightarrow \phi_k(U_k) \subseteq \mathbb{R}^m$ are diffeomorphisms onto their images. The pullback metric at $p \in U_j$ can be expressed in local coordinates as the following product of Jacobians:

$$G^{\varphi^i}(p) = J_{\varphi^i \circ \psi \circ \phi_j^{-1}}^\top J_{\varphi^i \circ \psi \circ \phi_j^{-1}} = J_{\psi \circ \phi_j^{-1}}^\top J_{\varphi^i}^\top J_{\varphi^i} J_{\psi \circ \phi_j^{-1}}$$

Now suppose we wish to change the local coordinates to use chart ϕ_k at $p \in U_j \cap U_k$ instead of ϕ_j . We define the following transition mapping:

$$\phi_k(U_j \cap U_k) \xrightarrow{\phi_k^{-1}} U_j \cap U_k \xrightarrow{\phi_j} \phi_j(U_j \cap U_k)$$

The transition function is $\phi_j \circ \phi_k^{-1}$, which maps between open subsets of \mathbb{R}^m , and we denote its Jacobian by $J_{kj}(p) \in \mathbb{R}^{m \times m}$. Here, unlike in the proof of proposition 4.1, the metric will change under this transformation. Denoting $\tilde{G}^{\varphi^i}(p)$ the new metric in local coordinates (associated with ϕ_k) at p :

$$\tilde{G}^{\varphi^i}(p) = J_{\varphi^i \circ \psi \circ \phi_j^{-1} \circ \phi_j \circ \phi_k^{-1}}^\top J_{\varphi^i \circ \psi \circ \phi_j^{-1} \circ \phi_j \circ \phi_k^{-1}} = J_{kj}^\top J_{\psi \circ \phi_j^{-1}}^\top J_{\varphi^i}^\top J_{\varphi^i} J_{\psi \circ \phi_j^{-1}} J_{kj}$$

which is not equal to $G^{\varphi^i}(p)$ in general. For notational clarity we will write $\mathbf{J}^i = J_{\varphi^i} J_{\psi \circ \phi_j^{-1}}$, so that

$$G^{\varphi^i}(p) = (\mathbf{J}^i)^\top \mathbf{J}^i, \quad \tilde{G}^{\varphi^i}(p) = J_{kj}^\top (\mathbf{J}^i)^\top \mathbf{J}^i J_{kj}$$

Now, the generalised eigenvalue problem in the new local coordinates becomes:

$$\tilde{G}^{\varphi^1}(p) \mathbf{v} = \lambda \tilde{G}^{\varphi^2}(p) \mathbf{v} \quad \Rightarrow \quad J_{kj}^\top (\mathbf{J}^1)^\top \mathbf{J}^1 J_{kj} \mathbf{v} = \lambda J_{kj}^\top (\mathbf{J}^2)^\top \mathbf{J}^2 J_{kj} \mathbf{v}.$$

Since the transition function is invertible, we can left-multiply by $J_{kj}^{-\top}$ to get:

$$(\mathbf{J}^1)^\top \mathbf{J}^1 \tilde{\mathbf{v}} = \lambda (\mathbf{J}^2)^\top \mathbf{J}^2 \tilde{\mathbf{v}}$$

where we let $\tilde{\mathbf{v}} = J_{kj} \mathbf{v}$. Thus, $\tilde{\mathbf{v}} / \|\tilde{\mathbf{v}}\|$ is a generalized eigenvector for the original local coordinates, with generalized eigenvalue λ . This tells us although the generalised eigenvectors may change under local coordinates, the generalised eigenvalues don't. Since the spectral ratio is only dependent on the generalised eigenvalues, MSA is independent of local coordinate changes. \square